processes

MDPI

Article

Geological Features, Paleosedimentary Environment, and Organic Matter Accumulation Mechanisms of the Lacustrine Shale Oil System: A Case Study of the Jurassic Dongyuemiao Member in the Sichuan Basin

Enze Wang [1,2,*], Yang Li [3], Tonglou Guo [4], Liang Xiong [4], Xiaoxia Dong [5], Tong Wang [5] and Kaibo Shi [2]

[1] State Key Laboratory of Shale Oil and Gas Enrichment Mechanisms and Effective Development, Beijing 102206, China
[2] School of Earth and Space Sciences, Peking University, Beijing 100871, China
[3] Petroleum Exploration and Production Research Institute, China Petrochemical Corporation, Beijing 102206, China
[4] Southwest Oil & Gas Company, China Petrochemical Corporation, Chengdu 610041, China
[5] Research Institute of Exploration and Development, China Petrochemical Corporation Southwest Oil and Gas Company, Chengdu 610041, China
* Correspondence: wangenze9939@163.com

Abstract: Lacustrine shale has garnered significant attention due to its significant resource potential. The Jurassic shale in the Sichuan Basin is an important target for lacustrine shale exploration in China. However, previous studies have predominantly focused on the Da'anzhai member of the Ziliujing Formation, and little attention has been paid to the shale of other strata. This paper aims to address this gap by investigating the Jurassic Dongyuemiao member in the Sichuan Basin. The study systematically characterizes the geological properties of the Dongyuemiao shale system, reconstructs the paleosedimentary environment, identifies the key factors influencing organic matter (OM) enrichment and physical properties, and assesses its resource potential through comparative analysis. Our results show that the Dongyuemiao shale was deposited in an oxic and semi-humid sedimentary environment characterized by intense weathering conditions. The enrichment of OM in the shale is primarily controlled by redox conditions and salinity, with redox conditions playing the most crucial role in OM accumulation. In terms of pore system characterization, clay mineral-associated pores dominate the pore types in the Dongyuemiao shale, while two types of organic matter-associated pores are also widely observed. The development of framework grain-associated pores is limited and only present in certain siliceous and carbonate minerals. The shales of the Dongyuemiao member and the Da'anzhai member exhibit slight differences in TOC content. However, the kerogen in the Dongyuemiao member displays higher hydrocarbon generation potential, and the Dongyuemiao shale exhibits more favorable pore structure parameters. Overall, the Dongyuemiao shale does not exhibit any significant disadvantages compared to the Da'anzhai shale. Therefore, it deserves greater attention in future exploration endeavors. The research findings presented in this paper provide a solid theoretical foundation for expanding the exploration scope of lacustrine shale in the Sichuan Basin.

Keywords: lacustrine shale; sedimentary environment; organic matter accumulation mechanism; Dongyuemiao member

Citation: Wang, E.; Li, Y.; Guo, T.; Xiong, L.; Dong, X.; Wang, T.; Shi, K. Geological Features, Paleosedimentary Environment, and Organic Matter Accumulation Mechanisms of the Lacustrine Shale Oil System: A Case Study of the Jurassic Dongyuemiao Member in the Sichuan Basin. *Processes* **2023**, *11*, 2638. https://doi.org/10.3390/pr11092638

Academic Editors: Jianhua Zhao, Guoheng Liu, Xiaolong Sun and Yuqi Wu

Received: 12 July 2023
Revised: 21 August 2023
Accepted: 23 August 2023
Published: 4 September 2023

1. Introduction

In China, significant achievements have been made in the exploration of lacustrine shale, with notable examples including the Paleogene Shahejie Formation in the Bohai Bay Basin, the Permian Lucaogou Formation in the Junggar Basin, the Cretaceous Qingshankou Formation in the Songliao Basin, and the Jurassic Ziliujing Formation in the

Sichuan Basin [1–13]. While marine shale formations such as the Longmaxi Formation have yielded significant industrial success [14–18], lacustrine shale formations exhibit stronger heterogeneity. Therefore, determining favorable exploration targets becomes a primary challenge for efficient exploration in lacustrine shale reservoirs.

Shale reservoirs are characterized as self-generating and self-storing reservoirs [19]. Consequently, the exploration potential of shale reservoirs primarily depends on the quality of the source rock and reservoir. The paleosedimentary environment plays a crucial role in organic matter (OM) enrichment, mineral composition, and pore system features. Consequently, the reconstruction of paleosedimentary environments holds significant importance for comprehending the mechanisms governing shale oil accumulation and identifying promising exploration targets [10,20–22]. In geological history, the Jurassic emerges as a paradigmatic greenhouse period characterized by warm and humid conditions. During this period, several organic-rich shale formations were deposited in China's petroliferous basins, including the Beipiao Formation of the Jinyang Basin, the Dameigou Formation of the Qaidam Basin, the Badaowan and Xishanyao Formations of the Junggar Basin, and the Ziliujing and Qianfoya Formations of the Sichuan Basin [23,24]. However, for different basins, the paleoenvironments and OM accumulation mechanisms of the Jurassic organic-rich shale are obviously different. Therefore, comprehensive and systematic research endeavors remain indispensable in elucidating these disparities.

The Jurassic Ziliujing Formation in the Sichuan Basin of southwestern China has obtained remarkable achievements, such as the YB21 well, which obtained a daily natural gas production of 50.7×10^4 m^3 in the Da'anzhai member of the Ziliujing Formation in the Yuanba oilfield [25]. However, the primary focus has been on the Da'anzhai member [26], while other strata have received limited attention. The Ziliujing Formation is characterized by two distinct lake basin expansion periods, resulting in the formation of two sets of black shale, namely the Da'anzhai member and the Dongyuemiao member [27]. The Da'anzhai shale has been extensively studied due to its large depositional area and abundant OM. However, the Dongyuemiao member may have an even larger depositional area than the Da'anzhai member, suggesting considerable potential for unconventional petroleum exploration [26]. To expand the exploration of Jurassic shale oil in the Sichuan Basin, this study focuses on the Dongyuemiao member in the Langzhong area. We use total organic carbon (TOC) analysis, X-ray diffraction (XRD), major and trace element analysis, field emission scanning electron microscopy (FE-SEM), and nitrogen adsorption (NA) analysis to characterize the core shale samples of the Dongyuemiao member. The research aims to systematically characterize the geological features of the Dongyuemiao shale, reconstruct the paleosedimentary environment, elucidate the mechanisms of OM enrichment, and identify the main controlling factors for physical properties. Additionally, a comparison is made with the Da'anzhai shale, and the resource prospects of the Dongyuemiao shale system are further discussed. The findings of this study will provide a theoretical basis for expanding the exploration scope of lacustrine shale in the Sichuan Basin.

2. Geological Setting

The Sichuan Basin, covering an area of approximately 18×10^4 km^2, is one of the most important petroliferous basins in SW China, with significant natural gas geological resources estimated at around 21.7×10^{12} m^3 [28,29]. In terms of tectonics, the Sichuan Basin is encircled by fold-thrust belts that encompass the Micang Shan and Daba Shan belts to the north, the Longmen Shan belt to the west, the east Sichuan belt to the east, and the southwest Sichuan belt to the south [30,31]. The Sichuan Basin was influenced by several tectonic movements, including the Caledonian (Late Ediacaran-Silurian), Hercynian (Devonian-Permian), Indosinian (Triassic), Yanshanian (Jurassic-Late Cretaceous), and Himalayan (Paleo-Quaternary) movements [32]. The Indosinian orogeny took place due to the convergence of the Indochina and South China blocks during the Triassic period as part of the tectonic process linked to the closure of the eastern branch of the Paleo-Tethyan [30,33,34]. The Sichuan Basin is located in the western sector of the South China block [31]. Following

the Indosinian movement, the Sichuan Basin underwent a transformation from a foreland basin in the Early Triassic to an intracontinental depression, and during the Jurassic period, lacustrine sedimentary systems prevailed. The Ziliujing Formation consists of four members, from bottom to top: the Zhenzhuchong, Dongyuemiao, Ma'anshan, and Da'anzhai members, with thicknesses of approximately 200–500 m [27]. The Dongyuemiao member represents a semi-deep to deep lake environment, characterized by the presence of black shale interbedded with thin bioclastic limestone and sandstone layers (Figure 1b). The source rocks within the Dongyuemiao member generally exhibit a thickness of 10–30 m. Given its extensive distribution and high TOC content, the Dongyuemiao shale presents a promising target for lacustrine shale exploration. The study area focuses on the Langzhong area, located in the central part of the Sichuan Basin.

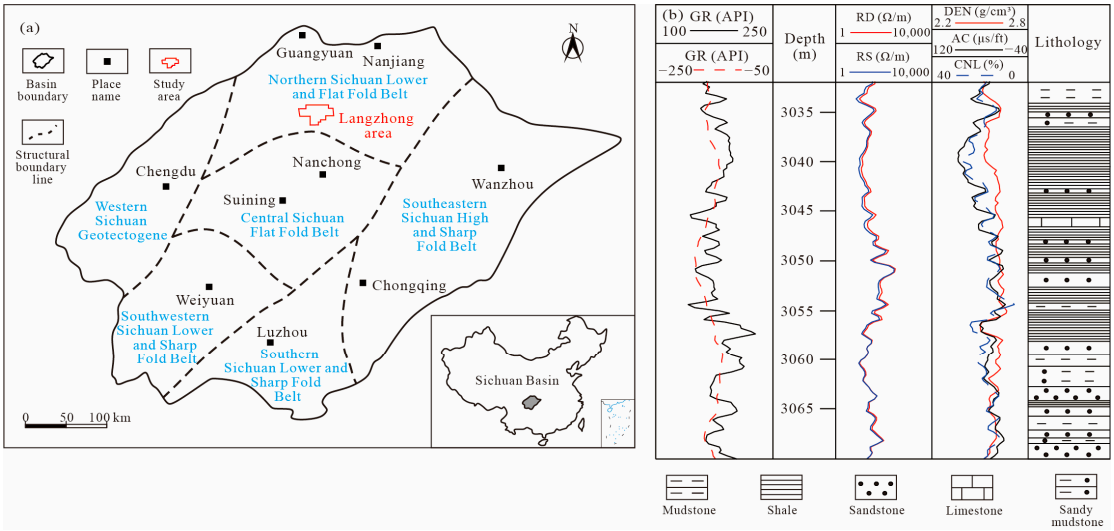

Figure 1. Comprehensive geological figure showing the location of the study area and features of strata column; (**a**) The location of the Langzhong area in the Sichuan Basin (modified from reference [8]); (**b**) The column of the Dongyuemiao member in the study area.

3. Data and Method

3.1. Data

The core samples used in this study were collected from the Dongyuemiao member in the LY1 well at the center of the Langzhong area. The LY1 well was drilled in 2020 to characterize the geological features of the Jurassic strata and provide guidance for exploration in the Jurassic lacustrine shale. In this study, we only selected the shale and mudstone samples in the borehole. Various experiments were conducted to investigate the geochemical and physical properties of the samples. The experiments involved include: TOC content, X-ray diffraction (XRD), helium porosity test, field emission scanning electron microscopy (FE-SEM) observation, nitrogen adsorption (NA) test, high pressure mercury injection (MIP), and major and trace element analysis. All experiments were conducted at the SINOPEC Wuxi Institute of Petroleum Geology.

For quantifying the TOC content, 21 samples were crushed to 200 mesh and treated with hydrochloric acid. After the inorganic carbon was removed, the samples were tested by a Leco CS-230 analyzer for TOC content. Major and trace element analysis was performed on 15 selected samples. Prior to the analysis, the OM was removed in a high-temperature oven, and a Rigaku 100E X-ray fluorescence spectrometer (XRF) was used for major element measurements. Trace element analysis was conducted using an Agilent 7500A inductively coupled plasma-mass spectrometry (ICP-MS) instrument after the samples were dissolved in a mixture of polytetrafluoroethylene, $HCIO_4$, HF, and HNO_3.

XRD measurements were conducted on 21 crushed samples, and the XRD data were obtained in an Ultima IV diffractometer operating at 40 kV and 40 mA. In order to reveal

physical properties and the pore system, 21 samples were Ar-ion polished for FE-SEM observation and helium porosity analysis. The FE-SEM observation instrument was a NanoFab ORION microscope. Subsequently, the samples were subjected to NA and MIP experiments by AutoPore 9520 and Micromeritics Tristar II 3020 surface area analyzers, respectively.

3.2. Methods

In this study, the paleoenvironment is primarily reconstructed by geochemical proxies. For most proxies, the principle is that the various elements tend to accumulate in sediments under different conditions. The element enrichment factor is a commonly used index to characterize the paleosedimentary environment, and the method to obtain this value is shown in Equation (1).

$$EF_X = (X/Al)_{sample}/(X/Al)_{PAAS} \quad (1)$$

where X and Al represent the elemental contents of X and Al, respectively, and PAAS is the content of each element in post-Archean Australian shale [35]. The enrichment factors of different elements can be calculated using Equation (1).

The chemical index of alteration (CIA) has been proposed for quantifying the chemical weathering condition; the principle of this index is that elements show various accumulation features under different weathering conditions [36]. The calculation method of the CIA is shown in Equation (2).

$$CIA = [(Al_2O_3)/(Al_2O_3 + Na_2O + K_2O + CaO^*)] \quad (2)$$

where CaO* in Equation (2) is the CaO content in silicate minerals [37], and CaO* can be obtained by Equation (3) and Equation (4) [38]. The content of CaO* is consistent with the content of Na_2O if the content of $CaO_\#$ is larger than Na_2O; otherwise, the content of CaO* equals the content of $CaO_\#$.

$$CaO_\# = CaO - 10 \times P_2O_5/3 \quad (3)$$

$$CaO^* = \begin{cases} Na_2O, & CaO_\# > Na_2O \\ CaO_\#, & CaO_\# < Na_2O \end{cases} \quad (4)$$

Based on the fundamental concept that diverse elements exhibit varying degrees of enrichment in sedimentary deposits under distinct climatic conditions, specific elements such as Fe, Mn, and Cr are predominantly enriched in settings characterized by higher humidity. Conversely, elements such as Ca, Mg, and Sr are commonly enriched in arid climatic conditions. Previous studies have introduced the concept of the C-value as a quantitative indicator for characterizing paleoclimate [39]. The calculation method is shown in Equation (5).

$$C - value = \sum(Fe + Mn + Cr + Ni + V + Co)/\sum(Ca + Mg + Sr + Ba + K + Na) \quad (5)$$

where Fe, Mn, Cr, Ni, V, Co, Ca, Mg, Sr, Ba, K, and Na are the elemental contents in sediment (ppm).

4. Results

4.1. Mineral Composition and OM Content

The mineral composition of the Dongyuemiao shale in the study area is depicted in Figure 2. Clay minerals are the dominant component, accounting for a distribution range of 29.3% to 63.1% and an average of 47.5%. Siliceous minerals, including quartz and feldspar, make up a slightly lower proportion compared to clay minerals. The content of siliceous minerals ranges from 21.1% to 55.6%, with an average of 42.5%. Quartz is the main siliceous mineral, while feldspar, specifically plagioclase, is present in lower quantities. The carbonate content in the Dongyuemiao shale is relatively low, with a range from trace

amounts (less than 1.0%) to 26.5% (average = 6.6%). The primary carbonate minerals identified are calcite (average = 4.4%) and siderite (average = 2.1%), while dolomite is rarely detected. The TOC content of Dongyuemiao shale exhibits strong heterogeneity, ranging from 0.15% to 2.90%, with an average of 0.99%.

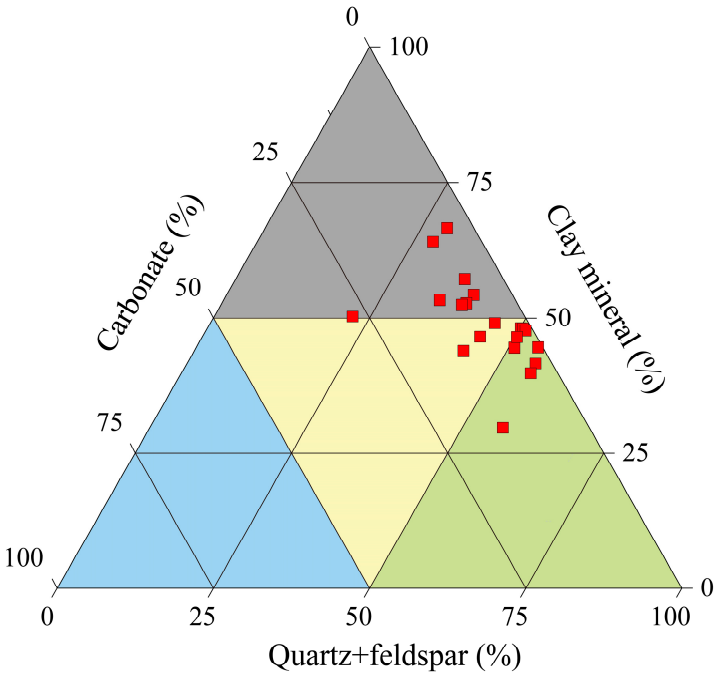

Figure 2. Ternary diagram showing the mineral composition of the Dongyuemiao shale of the study area.

4.2. Major and Trace Elements

The primary compound in the Dongyuemiao shale is SiO_2, with a distribution range of 42.4% to 63.9% (average = 54.6%). Al_2O_3 ranks as the second most abundant compound, ranging from 16.6% to 20.9% (average = 18.5%). Notably, the CaO content shows significant variation, ranging from 0.2 to 11.7% (average = 3.4%). Additionally, the contents of MgO (average = 1.7%), K_2O (average = 3.1%), and Fe_2O_3 (average = 5.9%) are generally greater than 1%. While the contents of Na_2O (average = 0.5%), P_2O_5 (average = 0.2%), and MnO (average = 0.1%) are generally less than 1% (Table 1).

Table 1. Major element data of the Dongyuemiao shale.

Depth (m)	TOC (%)	SiO_2 (%)	Al_2O_3 (%)	MgO (%)	Na_2O (%)	K_2O (%)	P_2O_5 (%)	TiO_2 (%)	CaO (%)	TFe_2O_3 (%)	MnO (%)
3034.16	1.55	52.48	20.74	1.89	0.53	3.66	0.20	0.78	2.65	6.00	0.04
3034.72	1.58	54.91	17.16	1.83	0.55	2.90	0.32	0.91	4.60	5.28	0.06
3036.55	1.71	56.84	18.49	1.77	0.60	2.91	0.13	0.90	3.11	5.49	0.04
3036.85	1.25	48.50	17.09	1.74	0.50	2.59	0.14	0.88	5.75	8.35	0.13
3037.12	1.85	57.60	19.17	1.81	0.61	2.86	0.18	0.97	1.66	5.50	0.05
3037.30	2.53	55.54	17.61	1.73	0.65	2.79	0.13	0.93	3.10	6.10	0.07
3038.00	2.72	58.87	17.42	1.75	0.63	2.82	0.32	0.93	1.38	6.22	0.07
3038.45	2.90	55.18	18.61	1.88	0.62	3.11	0.12	0.92	2.59	6.20	0.06
3040.00	1.06	55.10	18.56	1.82	0.55	3.13	0.19	0.92	1.78	6.72	0.08
3042.28	0.80	42.42	17.18	1.68	0.38	3.03	0.27	0.72	11.66	5.51	0.05
3042.93	1.56	49.10	20.60	1.92	0.42	3.70	0.27	0.88	4.34	5.94	0.04
3044.38	0.91	54.23	19.98	1.93	0.53	3.36	0.32	0.96	1.64	6.44	0.05
3051.05	1.06	53.88	16.56	1.60	0.58	2.51	0.31	0.91	5.87	6.10	0.12
3059.99	1.15	63.88	18.05	1.43	0.29	2.96	0.06	1.01	0.21	5.13	0.02
3064.14	0.11	61.11	20.86	1.17	0.42	3.74	0.05	0.92	0.20	3.41	0.01

Table 2 presents the trace element contents of the Dongyuemiao shale. The redox-sensitive elements, such as Mo and U, exhibit relatively low contents, typically below 5 ppm. Elements that characterize paleoproductivity, such as Ni, Cu, and Zn, show higher contents. Among them, Zn has the highest content, ranging from 86.7 ppm to 117.9 ppm (average = 102.8 ppm).

Table 2. Trace element data of the Dongyuemiao shale.

Depth (m)	TOC (%)	V (ppm)	Cr (ppm)	Co (ppm)	Ni (ppm)	Cu (ppm)	Zn (ppm)	Sr (ppm)	Mo (ppm)	Ba (ppm)	U (ppm)	Th (ppm)
3034.16	1.55	165.17	130.28	15.71	48.54	44.18	97.08	158.53	0.55	685.12	1.60	11.61
3034.72	1.58	136.13	122.15	15.05	44.06	44.73	86.68	148.09	0.70	566.06	2.05	14.35
3036.55	1.71	139.65	130.64	19.28	48.97	42.65	102.82	153.61	0.63	617.94	1.76	20.98
3036.85	1.25	130.72	126.10	21.39	58.83	40.44	94.85	180.55	0.79	547.72	1.97	13.87
3037.12	1.85	143.74	148.56	15.69	43.37	43.93	92.06	127.51	0.96	617.90	2.26	16.03
3037.30	2.53	136.38	122.05	14.98	38.67	37.80	94.34	151.39	1.04	661.35	1.92	11.56
3038.00	2.72	145.78	132.94	21.55	49.19	40.01	104.65	132.52	0.82	661.17	2.01	15.81
3038.45	2.90	148.42	127.95	18.58	50.32	42.73	112.96	143.60	0.83	656.58	2.28	13.86
3040.00	1.06	156.66	145.13	20.18	54.79	46.31	117.88	133.59	1.07	740.55	2.23	14.43
3042.28	0.80	135.53	119.74	14.86	44.63	44.71	110.55	294.23	0.62	656.79	1.91	10.49
3042.93	1.56	158.79	138.64	16.80	52.63	50.76	117.25	164.85	0.72	742.70	1.87	11.94
3044.38	0.91	164.65	145.42	22.67	60.76	54.80	114.90	137.38	0.75	707.80	1.94	15.00
3051.05	1.06	139.43	133.05	20.60	46.34	40.09	100.61	124.77	0.89	609.45	2.49	14.08
3059.99	1.15	135.40	134.21	14.55	47.28	31.31	103.87	82.20	0.47	479.49	2.37	14.89
3064.14	0.11	169.09	148.17	15.60	44.73	37.25	92.09	109.93	0.71	576.44	4.42	19.03

4.3. Pore System Characteristics

4.3.1. Pore System

To accurately depict the features of the pore system, we adopted the pore classification scheme proposed by previous studies [40,41]. The pore system of the Dongyuemiao shale is characterized by three main categories: organic matter-associated pores (OMPs), framework grain-related pores (FMPs), and clay mineral-related pores (CMPs). The geometric characteristics of these pores, which were characterized based on FE-SEM observations, are shown in Figure 3.

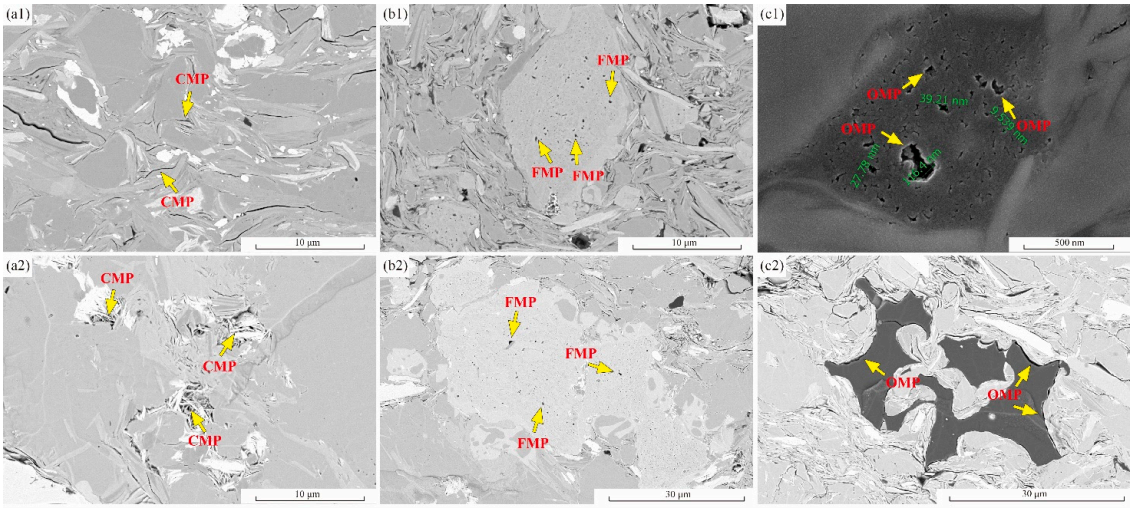

Figure 3. Pore system of the Dongyuemiao shale observed by FE-SEM: (**a1**) 3062.02 m, CMP; (**a2**) 3034.72 m, CMP; (**b1**) 3046.37 m, FMP; (**b2**) 3034.72 m, FMP; (**c1**) 3046.37 m, OMP; (**c2**) 3034.72 m, OMP.

In the Dongyuemiao shale, the pore system exhibits distinct features for different pore types. CMPs are primarily intergranular pores and fractures associated with clay minerals (primarily chlorite and illite). These pores are well-observed in the samples and typically have a nanoscale size with irregular shapes (Figure 3(a1,a2)). FMPs are also nanoscale in size and are mainly developed in calcareous and feldspar minerals. However, most of these pores are isolated and not interconnected with each other (Figure 3(b1,b2)). Two types of OMPs are identified. The first type is intragranular pores within the OM particles (Figure 3(c1)), which are typically nanoscale in size and exhibit irregular shapes. The second type of OMP is manifested as shrinkage fractures at the contact edges between OM particles and other minerals (Figure 3(c2)). These shrinkage fractures have larger pore sizes compared to intragranular pores but are relatively less abundant. In general, CMPs dominate the pore system, while two types of OMPs can also be observed. FMPs are poorly developed and are only found in some siliceous and carbonate minerals.

4.3.2. Physical Properties

The physical properties of the Dongyuemiao shale reservoir were quantitatively characterized using NA and MIP experiments. The results provide insights into the porosity, pore volume (PV), and specific surface area (SSA) of the shale.

The typical MIP and NA curves are shown in Figure 4. In the MIP test, the displacement pressure ranges from 43.04 to 43.06 MPa (average = 43.05 MPa). The mercury saturation initially increases slowly when the pressure is below a threshold of approximately 30 MPa. However, once the pressure exceeds the threshold, the mercury saturation rises rapidly. During the pressure decrease, the mercury withdrawal efficiencies of shale samples are generally not high and vary from 39.3 to 65.9% (average = 46.6%). In the NA experiment, the N_2 adsorption isotherm curve belongs to the type IV curve. When the relative pressure exceeds 0.8, the N_2 adsorption capacity increases rapidly. The curve also shows a hysteresis loop, which belongs to a mixed type of H2 and H3. This represents the presence of ink bottle- and slit-shaped pores.

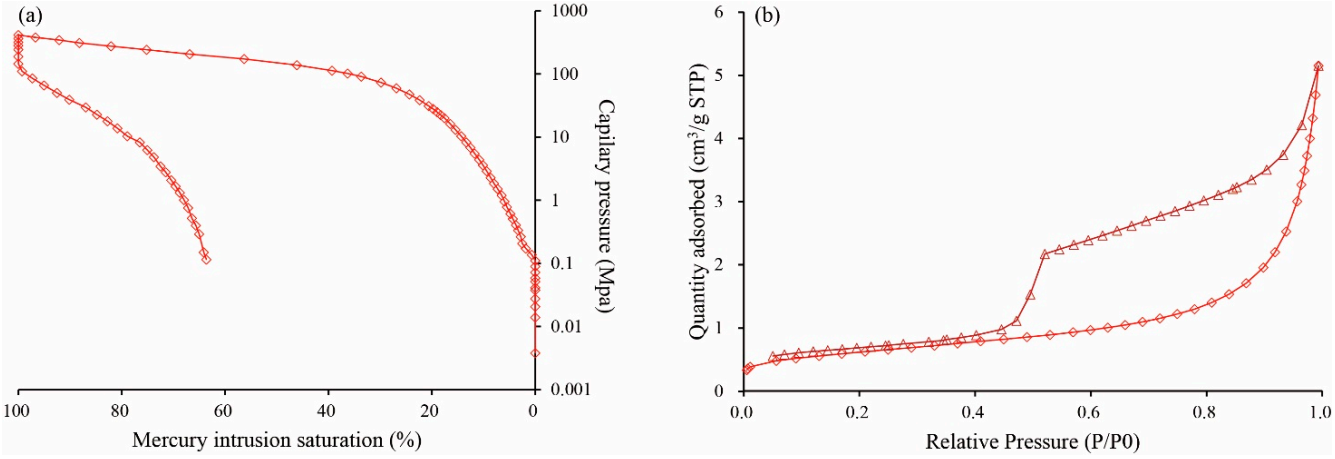

Figure 4. Typical MIP curve and NA adsorption–desorption curve of the Dongyuemiao shale. (**a**) The typical MIP curve; (**b**) The typical NA adsorption–desorption curve.

Based on the two experiments, the PV ranges of the Dongyuemiao shale in the study area range from 0.0052 to 0.0170 cm^3/g (average = 0.0118 cm^3/g), and the SSA varies from 1.29 to 7.12 m^2/g (average = 3.79 m^2/g). According to the helium porosity test, the porosity ranges from 1.4 to 5.3%, with an average of 3.7%.

5. Discussion

5.1. Paleosedimentary Environment and Organic Matter Accumulation Mechanism

5.1.1. Paleoclimate and Weathering Conditions

The paleoclimate and weathering conditions of the Dongyuemiao shale can be assessed through several geochemical proxies, including the CIA value, K_2O/Rb ratio, Ln (Al_2O_3/Na_2O) ratio, and C-value [26,38,42]. The CIA values falling within the ranges of 80–100, 70–80, and 50–70 correspond to strong, moderate, and weak weathering, respectively [37,43]. The C-values falling below 0.2, within the range of 0.2 to 0.4, 0.4 to 0.6, 0.6 to 0.8, and exceeding 0.8 are indicative of paleoclimatic environments characterized as arid, semi-arid, semi-arid to semi-humid, semi-humid, and humid, respectively [39]. The CIA value ranges from 81.1 to 84.7 (average = 82.1), and the C-value varies from 0.32 to 0.97 (average = 0.69). The CIA values suggest that the weathering intensity of the shale remains relatively consistent, indicating a strong weathering condition during the deposition period of the Dongyuemiao member. Furthermore, the C-value corroborates this interpretation, highlighting a semi-humid depositional setting (Figure 5). When integrating these proxies, it becomes evident that the Dongyuemiao shale was deposited in a semi-humid environment with strong weathering. Notably, an improvement in K_2O/Rb and Ln (Al_2O_3/Na_2O) ratios reflects the intensified weathering condition [38,42]. The ranges of K_2O/Rb and Ln (Al_2O_3/Na_2O) ratios within the Dongyuemiao member are 170.3 to 194.2 (average = 183.8) and 3.3 to 4.1 (average = 3.6), respectively. These values collectively underscore the relatively stable and sustained nature of the weathering conditions during the Dongyuemiao period.

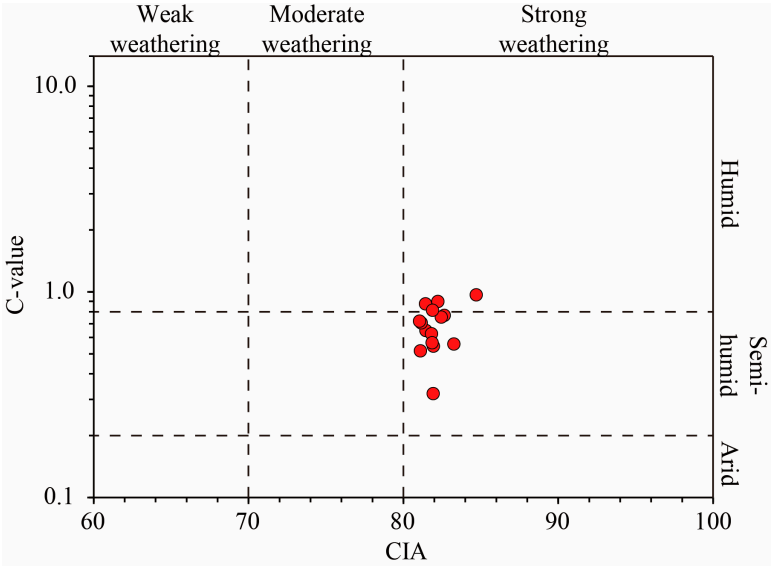

Figure 5. C-value and CIA diagram to describe the paleoclimate and weathering conditions of the Dongyuemiao shale.

5.1.2. Redox Conditions

The redox condition is a crucial factor influencing the OM accumulations [44]. The contents and ratios of redox-sensitive elements are reliable proxies for representing redox conditions. The Mo element, for example, is generally enriched in sediments under anoxic conditions. Mo contents less than 25 ppm, between 25 and 100 ppm, and greater than 100 ppm are indicative of oxic, dysoxic, and anoxic environments, respectively [45]. Similarly, a high Mo_{EF} often indicates a relatively reductive environment. Additionally, ratios of redox-sensitive elements (such as V/Cr, Ni/Co, and U/Th) [46] are effective proxies for assessing redox conditions. The Mo content ranges from 0.47 to 1.07 (average = 0.77), and the Mo_{EF} varies from 0.34 to 0.76 (average = 0.54), indicating that the Dongyuemiao shale was predominantly deposited in an oxic environment. The ratios of redox-sensitive

elements, including V/Cr, Ni/Co, and U/Th, range from 0.97 to 1.27 (average = 1.10), 2.25 to 3.25 (average = 2.77), and 0.08 to 0.23 (average = 0.15), respectively. These ratios further support the interpretation of an oxic depositional environment for the Dongyuemiao member (Figure 6). The Cu/Zn ratio can be used as a reliable proxy for characterizing the redox condition [47]. The Cu/Zn ratio of the shale of the Dongyuemiao member ranges from 0.30 to 0.52 (average = 0.42), which reflects the oxic condition during the sedimentary process. Previous studies have shown that Corg/P values less than 50, between 50 and 100, and greater than 100 represent oxic, suboxic, and anoxic depositional environments, respectively [48]. The Corg/P value of the Dongyuemiao shale ranges from 12.5 to 142.7 (average = 54.6), indicating significant fluctuations in the redox conditions and a transition from oxic to anoxic environments. This discrepancy with the results obtained from the ratios and content of redox-sensitive elements suggests that using fixed criteria for evaluating redox conditions based on geochemical proxies may have limitations [49]. Considering multiple geochemical proxies, we conclude that the Dongyuemiao shale in the study area was primarily deposited in an oxic sedimentary environment.

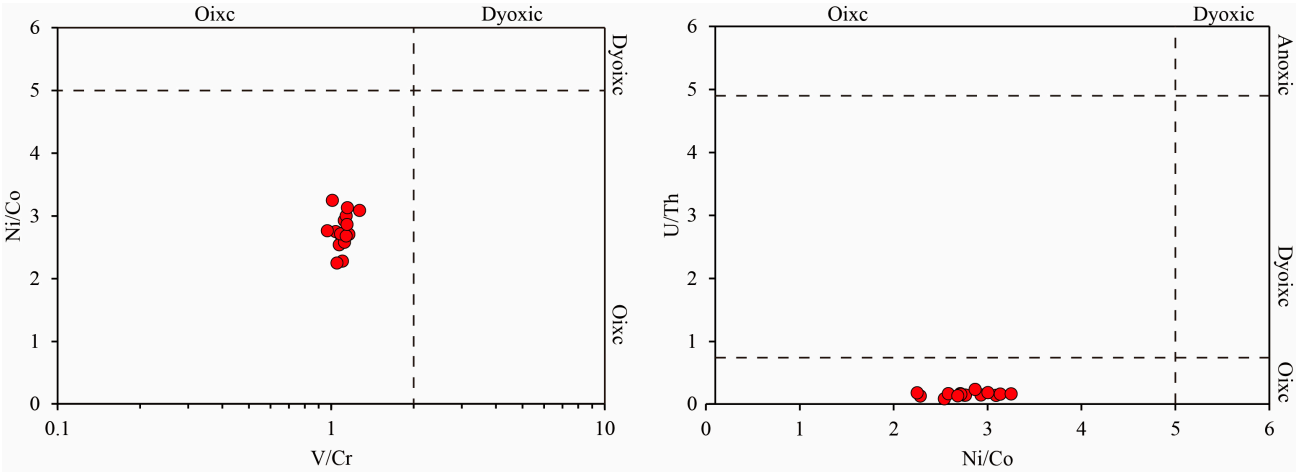

Figure 6. Cross-plot showing the redox condition of the Dongyumiao shale.

5.1.3. Salinity Condition

The differing solubilities of $BaSO_4$ and $SrSO_4$ render the Sr/Ba ratio a valuable indicator of paleo-salinity. Wei and Algeo [50] suggest the Sr/Ba ratios less than 0.2, 0.2 to 0.5, and greater than 0.5 reflect freshwater, brackish water, and marine salinities, respectively. However, it is essential to note that the accuracy of the Sr/Ba ratio as a salinity proxy may be compromised in samples containing over 4% CaO. In the case of the Dongyuemiao shale, the CaO content spans from 0.2 to 11.7 (average = 3.4), prompting the exclusion of five samples from the Sr/Ba ratio analysis. This adjustment yields an average CaO content of 1.8% for the remaining samples. The Sr/Ba ratio of the Dongyuemiao shale ranges from 0.17 to 0.25 (average = 0.21), which reflects that the shale of the Dongyuemiao member was deposited in a brackish to freshwater condition. The MgO/Al_2O_3 ratio has been widely used as a proxy for estimating salinity in sedimentary environments. A higher MgO/Al_2O_3 ratio indicates higher salinity conditions, while a lower ratio suggests lower salinity conditions [26]. The MgO/Al_2O_3 ratio of the Dongyuemiao shale ranges from 0.06 to 0.11 (average = 0.09). In comparison with earlier data, this finding further corroborates the conclusion derived from the Sr/Ba ratio [26].

5.1.4. Terrigenous Debris Influx and Primary Productivity

Certain lithogenic elements, including Al, Si, Ti, and Zr, serve as robust proxies of terrigenous debris influx [51,52]. Zr is commonly associated with the heavy mineral zircon, while Al is primarily found in clay mineral fractions. Ti is present in both silt- and sand-sized particles as well as in clay fractions. Similarly, Si is present in quartz and clay

minerals [35]. Consequently, ratios such as Si/Al, Zr/Al, and Ti/Al can provide insights into the clastic sediment component. An elevation in Zr/Al and Ti/Al ratios signifies increased eolian detrital input, while an increase in Si/Al ratio reflects enhanced fluvial delivery of clastic material [52,53]. The distribution ranges for the Si/Al, Zr/Al, and Ti/Al ratios within the Dongyuemiao shale are 2.10 to 3.12 (average = 2.61), 5.5 × 10^{-4} to 10.0 × 10^{-4} (average = 7.6 × 10^{-4}), and 0.043 to 0.063 (average = 0.055), respectively. Importantly, these three parameters exhibit notable correlations (Figure 7), reflecting that the Dongyuemiao member experienced a consistent weathering condition and sediment provenance [42].

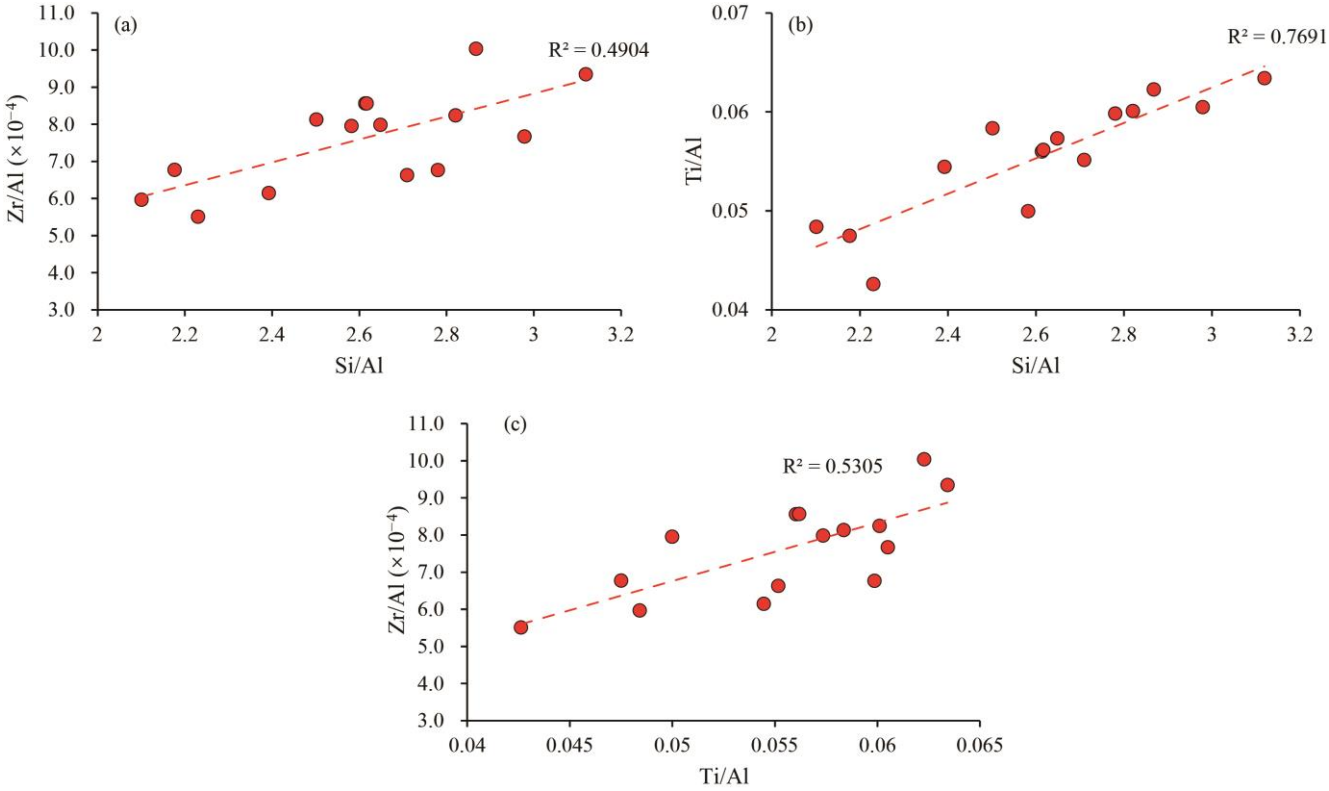

Figure 7. Cross plot showing the correlations of proxies representing the terrigenous debris influx of the Dongyumiao shale. (**a**) The relationships between Si/Al and Zr/Al; (**b**) The relationships between Si/Al and Ti/Al; (**c**) The relationships between Ti/Al and Zr/Al.

Cu, Ni, and Zn contents serve as indicators to assess primary productivity patterns [42,52,54]. These elements are essential micro-nutrients participating in biological metabolism, and they are transported to sediments in conjunction with sedimentary OM in the form of organometallic complexes [52,54]. To eliminate the impact of terrigenous debris influx, we employ the Al-normalized Ni, Cu, and Zn values of the Dongyuemiao shale to characterize primary productivity levels. Generally, elevated Cu/Al, Ni/Al, and Zn/Al ratios signify high primary productivity [42,52]. The ranges of the Cu/Al, Ni/Al, and Zn/Al ratios of the Dongyuemiao shale are 3.3 × 10^{-4} to 5.2 × 10^{-4} (average = 4.4 × 10^{-4}), 8.3 × 10^{-4} to 12.1 × 10^{-4} (average = 10.5 × 10^{-4}), and 4.0 × 10^{-4} to 6.5 × 10^{-4} (average = 5.0 × 10^{-4}), respectively. Similarly, these proxies exhibit strong correlations (Figure 8), but display no significant correlations with TOC content (Figure 9). These findings suggest relatively low primary productivity during the deposition of the Dongyuemiao period. Moreover, considering the Cu/Al ratio as an example, the Cu/Al ratio in the Dongyuemiao shale is notably lower than that of the PAAS (0.0005) [35]. This observation further supports the inference of relatively low primary productivity in the Dongyuemiao shale.

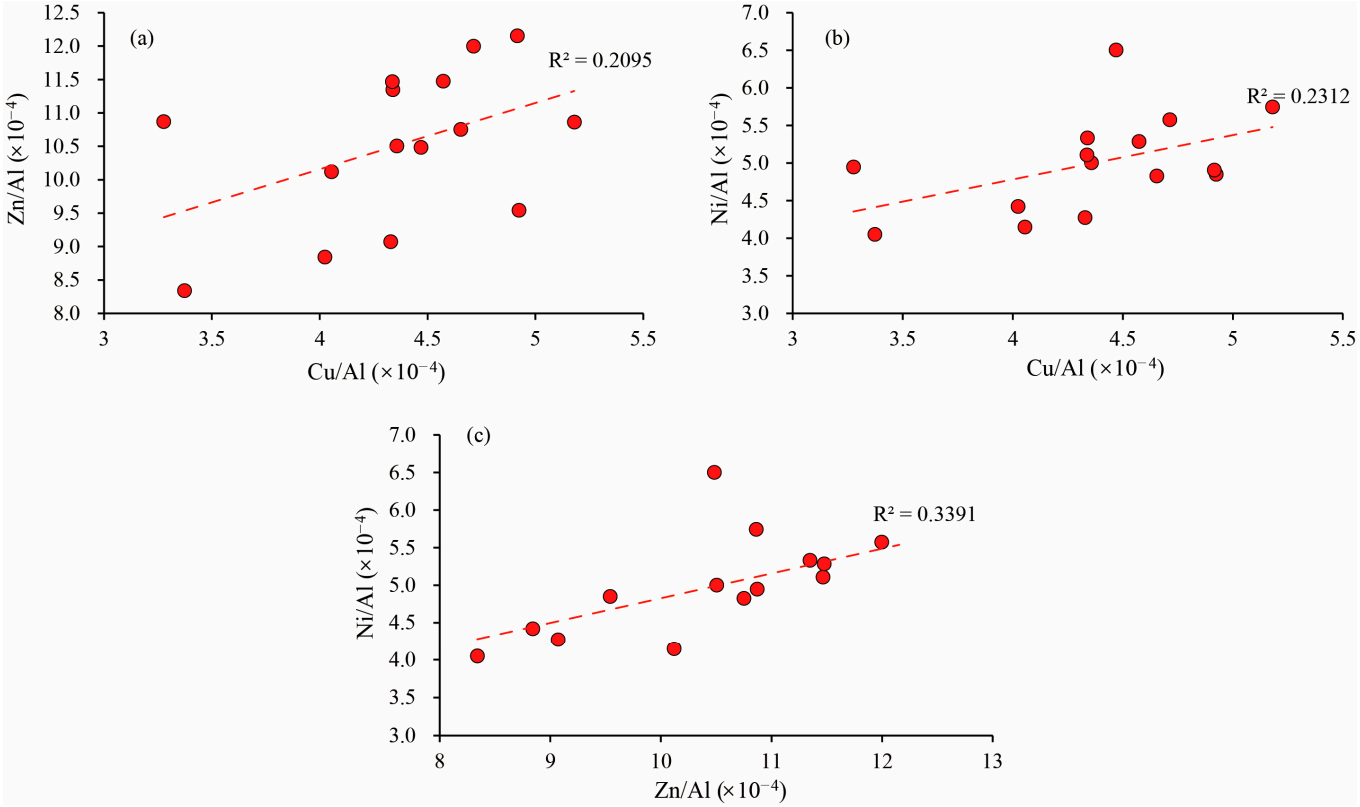

Figure 8. Cross plot showing the correlations of proxies representing the primary productivity of the Dongyumiao shale. (**a**) The relationships between Cu/Al and Zn/Al; (**b**) The relationships between Cu/Al and Ni/Al; (**c**) The relationships between Zn/Al and Ni/Al.

5.1.5. OM Accumulation Mechanisms

The correlation analysis between TOC content and paleoenvironmental proxies is presented in Figure 9. Among the proxies indicative of redox conditions, the most pronounced correlation is observed with TOC content, underscoring the pivotal role of redox conditions in governing OM accumulation in the Dongyuemiao shale. Despite the Dongyuemiao shale generally exhibiting a salinity range indicative of freshwater to brackish conditions, potentially insufficient to induce substantial water column stratification, salinity also demonstrates a positive correlation with TOC content.

Terrigenous debris influx exerts a dual influence on OM accumulation. On the one hand, the terrestrial debris influx has the capacity to adsorb OM from the water column, facilitating its rapid transport to the seafloor. This process effectively reduces OM loss during the deposition process [55,56]. Conversely, if the supply of OM remains constant, an augmentation in terrigenous debris influx could lead to the dilution of primary productivity, resulting in a reduction in OM content [57]. In the present study, a clear correlation between the proxy reflecting terrigenous debris influx and the TOC content within the Dongyuemiao shale is not readily apparent. This lack of a straightforward relationship may arise from the interplay of both positive (improves deposition rate) and negative (dilutes primary productivity) factors. Notably, the negative correlation observed between the Si/Al ratio and the Cu/Al ratio (Figure 10) suggests that the influx of terrigenous debris might indeed contribute to the attenuation of primary productivity. Consequently, the intricate interplay of these opposing influences gives rise to a complex situation where the correlation between terrigenous debris influx and TOC content remains less evident.

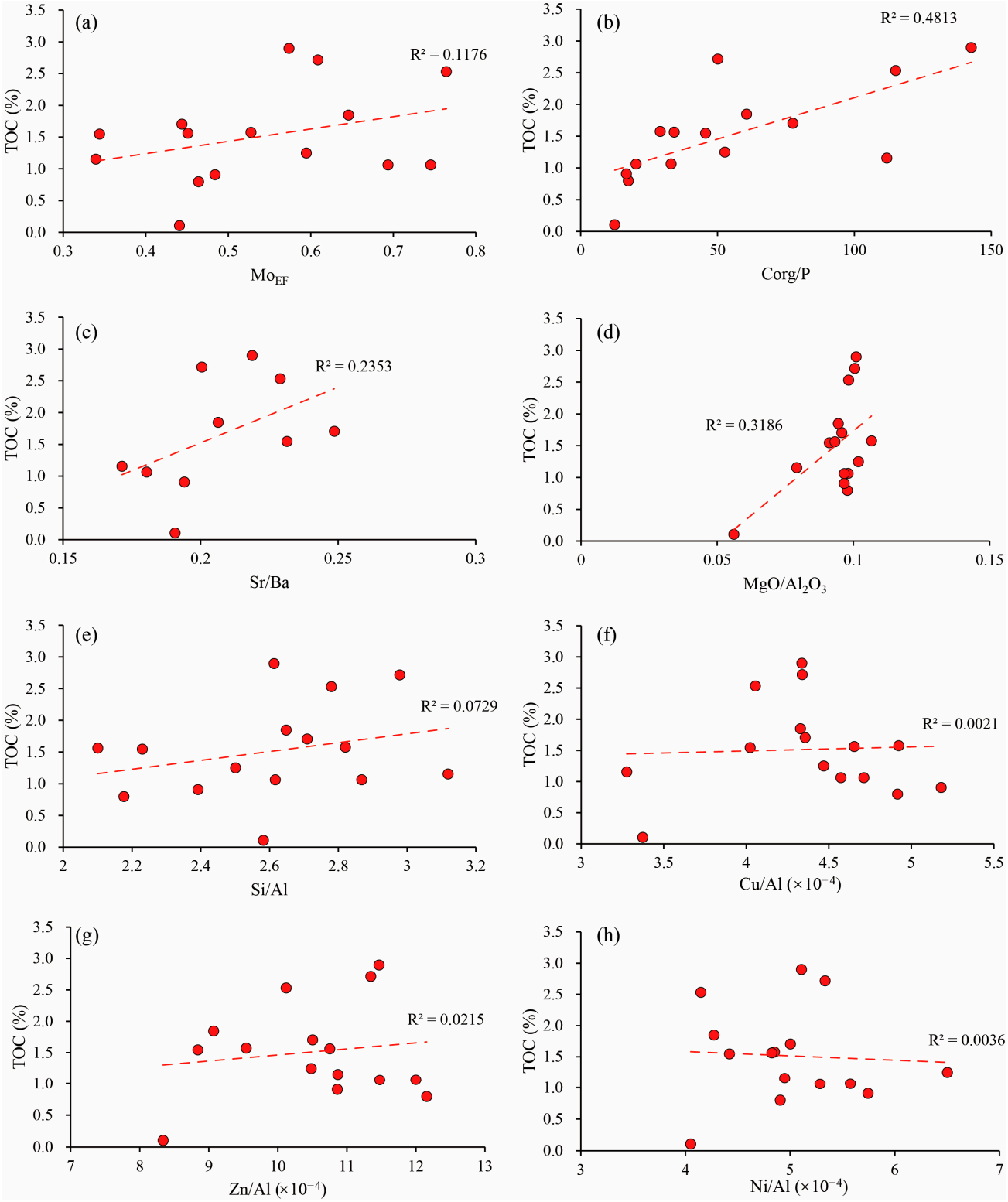

Figure 9. OM accumulation mechanisms of the Dongyuemiao shale. (**a**) The relationships between Mo_{EF} value and TOC content; (**b**) The relationships between Corg/P ratio and TOC content; (**c**) The relationships between Sr/Ba and TOC content; (**d**) The relationships between MgO/Al_2O_3 and TOC content; (**e**) The relationships between Si/Al and TOC content; (**f**) The relationships between Cu/Al and TOC content; (**g**) The relationships between Zn/Al and TOC content; (**h**) The relationships between Ni/Al and TOC content.

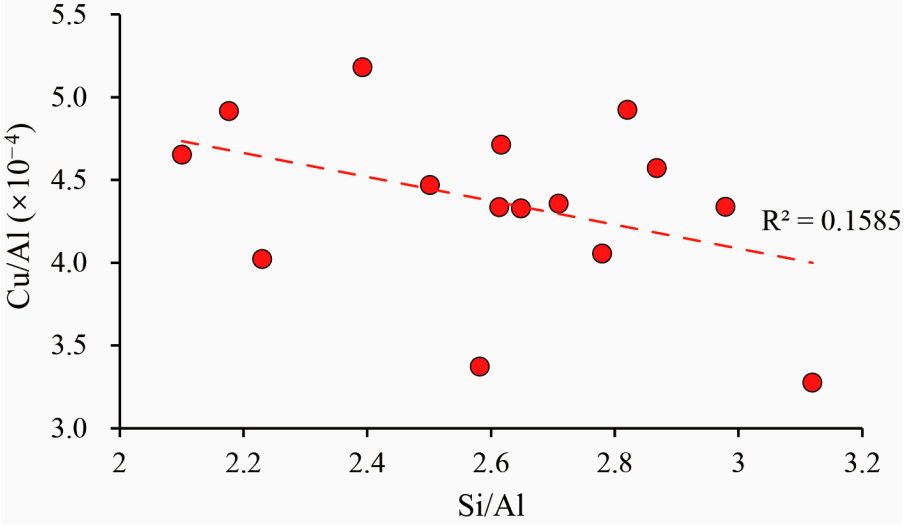

Figure 10. Correlations between the terrigenous debris influx proxy and the primary productivity proxy of the Dongyuemiao shale.

The weak correlation observed between the proxy representing primary productivity and TOC content in the Dongyuemiao shale suggests that primary productivity is not a significant factor influencing OM enrichment. This can be attributed to the relatively limited variability observed in the proxies representing primary productivity compared to those representing redox conditions. In conclusion, the enrichment of OM in the Dongyuemiao shale is primarily controlled by redox conditions and salinity. The redox condition plays the most critical role in OM enrichment, while primary productivity has minimal influence on the TOC content.

5.2. Controlling Factors for Physical Properties

We adopted the pore size classification proposed by Yang et al. [58] specifically for lacustrine shale, as the pore sizes observed in the Dongyuemiao shale varied significantly. The classification includes micropores (1–10 nm), transitional pores (10–100 nm), mesopores (100–1000 nm), and macropores (more than 1000 nm). The pore structure parameters corresponding to different pore sizes are shown in Table 3. Micropores contribute the most to SSA, accounting for a range of 56.8 to 84.8% (average = 73.2%), while transitional pores contribute the most to PV, ranging from 42.6 to 60.9% (average = 51.2%). Mesopores and macropores have relatively low influences on pore structure parameters.

Table 3. Pore structure parameters of the Dongyuemiao shale.

Parameters	Micropre (1–10 nm)	Proportion (%)	Transitional Pore (10–100 nm)	Proportion (%)	Mesopore (100–1000 nm)	Proportion (%)	Macropore (>1000 nm)	Proportion (%)
PV (cm^3/g)	0.0007–0.0048 (0.0027)	11.5–33.3 (23.0)	0.0022–0.0092 (0.0061)	42.2–60.9 (51.2)	0.0015–0.0031 (0.0022)	13.3–28.2 (19.3)	0.0005–0.0015 (0.0007)	3.6–11.3 (6.5)
SSA (m^2/g)	0.7357–6.0336 (2.8237)	56.8–84.8 (73.2)	0.3088–1.4340 (0.9144)	14.6–39.5 (25.3)	0.0308–0.0774 (0.0481)	0.7–3.6 (1.5)	0.0004–0.0014 (0.0007)	<0.1

The main controlling factors for the physical properties of the Dongyuemiao shale reservoir are depicted in Figure 11. There is a significant positive correlation between clay mineral content and physical properties, indicating the dominant role of CMPs in the pore system. Additionally, TOC content also exhibits a positive correlation with physical properties, suggesting the OMP plays an important role in the pore system. However, there is generally a significant negative correlation between brittle mineral content and physical properties. This can be attributed to several reasons. First, FMPs are poorly developed in the Dongyuemiao shale, and an increase in brittle mineral content does not significantly contribute to the pore system through FMPs. Second, the increase in brittle

mineral content is inevitably accompanied by a decrease in clay mineral content, leading to a loss of the material basis for CMP development. Finally, although a higher content of brittle minerals typically improves the compaction resistance of the reservoir, in the case of the Dongyuemiao shale, the low content of brittle minerals prevents the formation of an effective solid framework to protect the pores. Consequently, there is a negative correlation between brittle mineral content and physical properties in the Dongyuemiao shale.

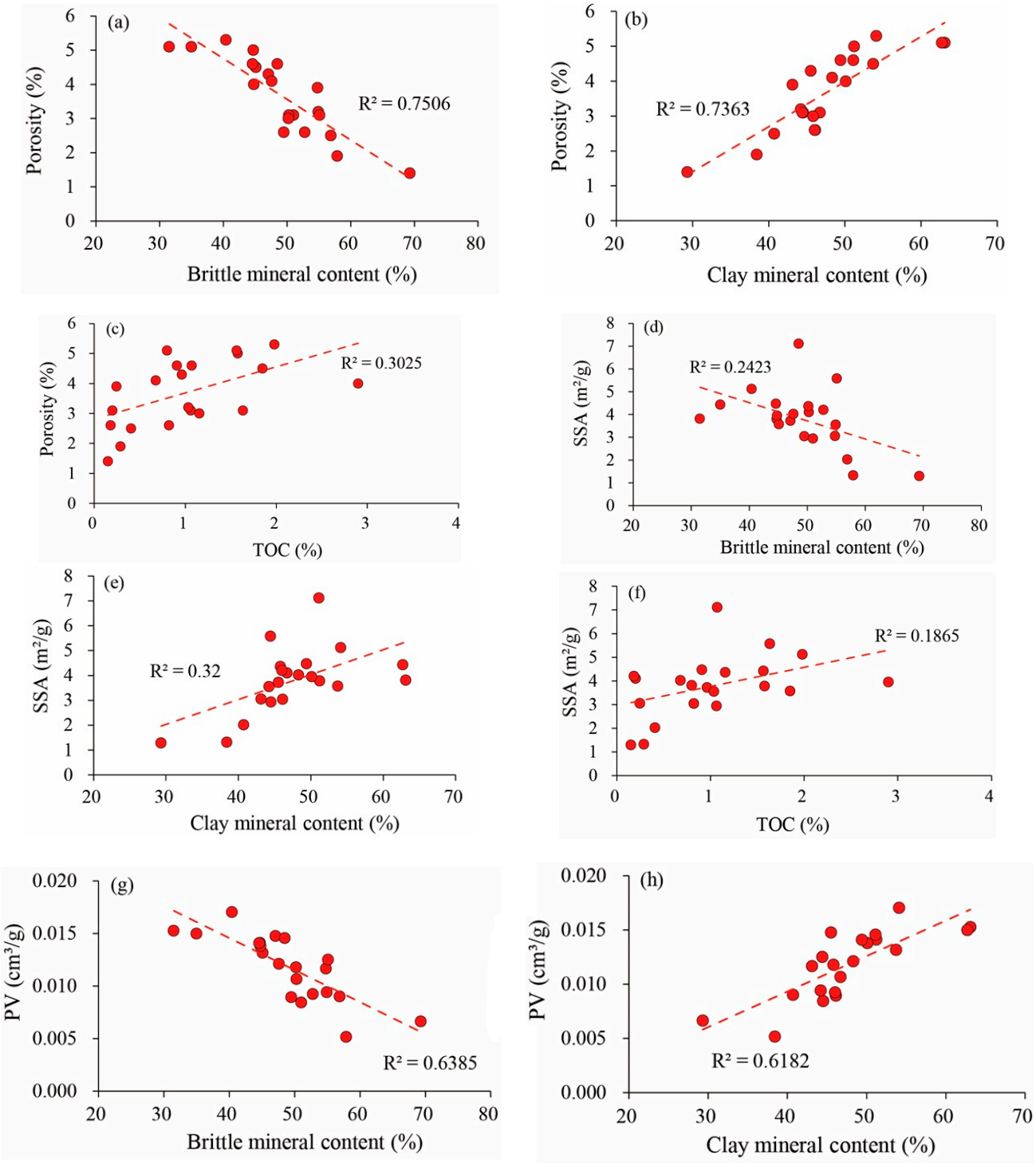

Figure 11. *Cont.*

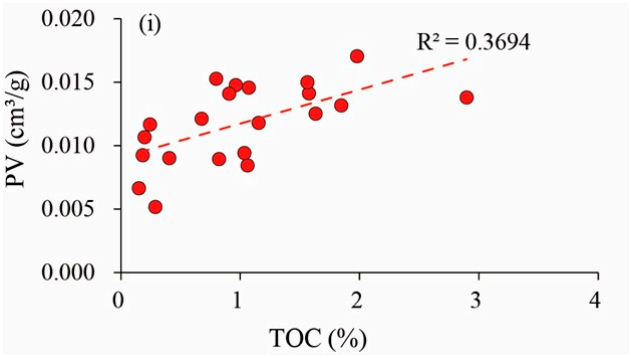

Figure 11. Controlling factors for the physical properties of the Dongyuemiao shale. (**a**) The relationships between brittle mineral content and porosity; (**b**) The relationships between clay mineral content and porosity; (**c**) The relationships between TOC content and porosity; (**d**) The relationships between brittle mineral content and SSA; (**e**) The relationships between clay mineral content and SSA; (**f**) The relationships between TOC content and SSA; (**g**) The relationships between brittle mineral content and PV; (**h**) The relationships between clay mineral content and PV; (**i**) The relationships between TOC content and PV.

To analyze the main pore types at different pore sizes, we examined the correlation between PV and SSA at various pore sizes (Figures 12 and 13). Brittle mineral content shows a negative correlation with the pore structure parameters of all pore sizes, indicating a weak contribution of FMPs to the pore system. Clay mineral content exhibits a significant correlation with pore structure parameters, suggesting a wide distribution range of CMPs across various pore sizes (nano-sized to micro-sized). OMPs show correlations with pore structure parameters of transitional pores and mesopores, as indicated by relatively high determination coefficients. This indicates that OMPs predominantly contribute to pore sizes ranging from 10 to 1000 nm. It is worth noting that the determination coefficients between TOC content and pore structure parameters of micropores are smaller compared to transitional pores and mesopores. This suggests that the number of OMPs with pore sizes in the range of 1 to 10 nm is limited in the Dongyuemiao shale, in contrast to the marine Longmaxi shale. This observation implies that the development of OMPs is controlled by kerogen type.

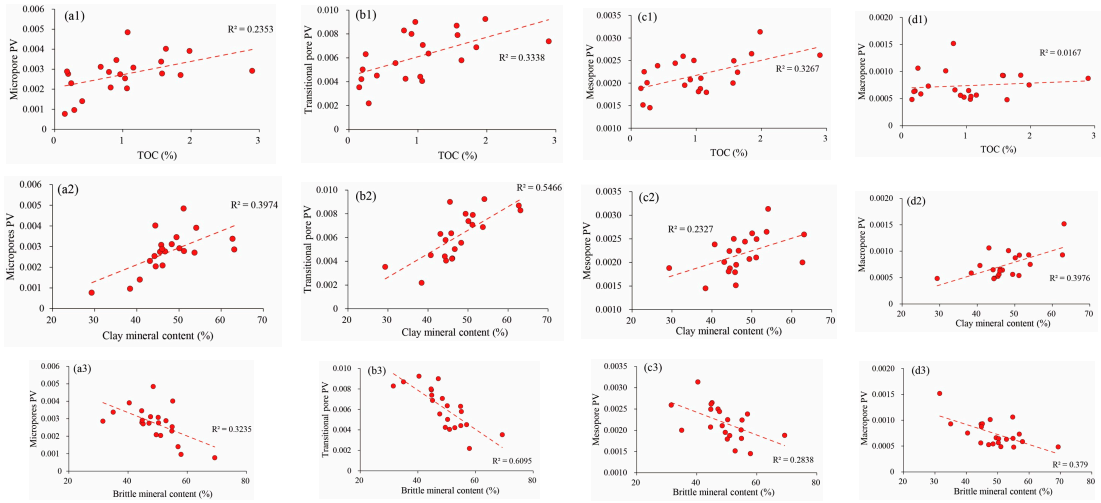

Figure 12. Correlations of mineral compositions and TOC content with PVs of different sizes of pores. (**a1–a3**) show the relationships between PVs of micropores and mineral composition (TOC content); (**b1–b3**) show the relationships between PVs of transitional pores and mineral composition (TOC content); (**c1–c3**) show the relationships between PVs of mesopores and mineral composition (TOC content); (**d1–d3**) show the relationships between PVs of macropores and mineral composition (TOC content).

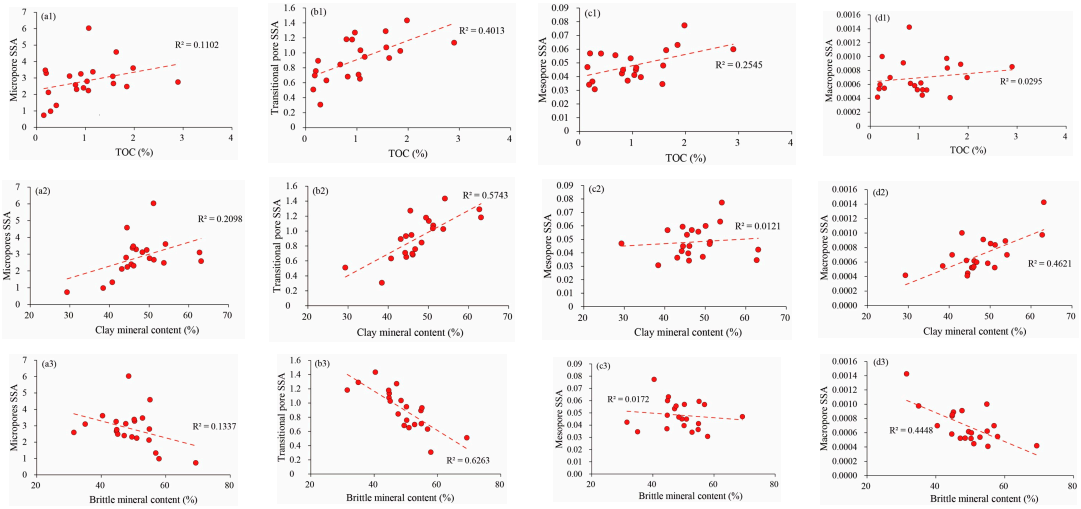

Figure 13. Correlations of mineral compositions and TOC content with SSA of different size pores. (**a1**–**a3**) show the relationships between SSAs of micropores and mineral composition (TOC content); (**b1**–**b3**) show the relationships between SSAs of transitional pores and mineral composition (TOC content); (**c1**–**c3**) show the relationships between SSAs of mesopores and mineral composition (TOC content); (**d1**–**d3**) show the relationships between SSAs of macropores and mineral composition (TOC content).

5.3. Comparison of Geological Features of Lacustrine Shale Petroleum Systems

To better understand the exploration potential of the Jurassic Dongyuemiao member in the Sichuan Basin, we compared the geological characteristics of the Dongyuemiao and Da'anzhai shales. The data for the Da'anzhai shale is referenced from Wang et al. [59]. The key findings regarding geological features are summarized in Table 4.

Table 4. Geological feature comparison of the different shale petroleum systems of the Langzhong area.

Member	TOC (%)	Paleoenvironment			Pore System			
		Weathering	Salinity Condition	Redox Condition	Porosity	PV	SSA	Pore Type
Dongyuemiao	0.11–2.90 (1.51)	Strong (average CIA 82.1)	Freshwater to brackish (average Sr/Ba 0.21)	Oxic environment (average Mo_{EF} 0.54)	1.4–5.3 (3.7)	0.0052–0.0170 (0.0118)	1.29–7.12 (3.79)	Mainly CMPs, OMPs have an impact on physical properties.
Da'anzhai	0.1–3.63 (1.56)	Moderate to strong (average CIA 81.7)	Freshwater to brackish (average Sr/Ba 0.21)	Oxic environment (average Mo_{EF} 0.80)	1.3–6.5 (4.5)	0.0057–0.0157 (0.0110)	0.79–5.50 (2.40)	Mainly CMPs, the development of OMPs is obviously different and has no obvious influence on physical properties.

Note: Minimum-maximum (average value).

The TOC content ranges of the Dongyuemiao and Da'anzhai shales are 0.11 to 2.90% (average = 1.51%) and 0.10 to 3.63 (average = 1.56%), respectively. The Da'anzhai shale exhibits a wider distribution range and a slightly higher average TOC content compared to the Dongyuemiao shale. One of the significant differences between the two shale members lies in their paleosedimentary environments, leading to variations in the mechanisms of OM enrichment. Specifically, salinity plays contrasting roles in the two members. As discussed earlier, high salinity favors OM preservation in the Dongyuemiao shale. In contrast, salinity has an adverse effect on OM accumulation in the Da'anzhai member, likely influenced by the Toarcian Oceanic Anoxic Event (T-OAE) that impacted the sedimentary environment [59]. These findings suggest that the same factors can have different impacts on OM enrichment due to variations in the sedimentary background.

From the perspective of the pore system, the porosity distributions of the Dongyuemiao and Da'anzhai shales range from 1.4 to 5.3% (average = 3.7%) and 1.3 to 6.5% (average = 4.5%), respectively. The porosity of the Da'anzhai shale is slightly higher than that of the Dongyuemiao shale. However, when considering pore structure parameters such as PV and SSA, the Dongyuemiao shale exhibits slightly higher values compared to the Da'anzhai shale. These differences in physical properties are attributed to variations in pore types. While CMPs dominate the pore system in both shales, the contribution of OMPs to the physical properties should not be overlooked. The Dongyuemiao shale's kerogen contains a higher hydrogen component compared to the Da'anzhai member [60]. As a result, the development of OMPs in the Dongyuemiao shale is more pronounced, leading to higher SSA.

In summary, from the perspective of source rocks, the TOC content of the Dongyuemiao member and the Da'anzhai member exhibit slight differences due to variations in sedimentary environments. However, the kerogen in the Dongyuemiao shale contains a higher hydrogen component, indicating higher hydrocarbon generation potential. From the perspective of the pore system, although the porosity of the Dongyuemiao member is slightly lower than that of the Da'anzhai member, it possesses better pore structure parameters. Therefore, the Dongyuemiao shale does not show any significant disadvantages compared to the Da'anzhai shale, and it deserves more attention in future exploration efforts.

6. Conclusions

In this study, the lacustrine shale of the Dongyuemiao member in the Langzhong area of the Sichuan Basin was investigated. The geological characteristics of the Dongyuemiao shale system were thoroughly examined, including the reconstruction of the paleosedimentary environment and the identification of the main controlling factors for OM enrichment and physical properties. Finally, a comparison was made to assess the petroleum exploration potential of the Dongyuemiao shale. The main conclusions derived from this study are as follows:

1. The Dongyuemiao shale was deposited in an oxic and semi-humid environment with strong weathering. The enrichment of OM in the shale is primarily influenced by the redox condition and salinity. The redox condition plays the most critical role in OM accumulation.
2. Based on the analysis of pores and minerals, three types of pores were identified in the Dongyuemiao shale: CMPs, OMPs, and FMPs. CMPs are the dominant pore type, while two types of OMPs were also observed. FMPs, on the other hand, are poorly developed and limited to certain siliceous and carbonate minerals.
3. Although the TOC content of the Da'anzhai shale is slightly higher than that of the Dongyuemiao shale, the kerogen in the Dongyuemiao shale contains a higher hydrogen component, indicating greater hydrocarbon generation potential. Additionally, the Dongyuemiao shale exhibits better pore structure parameters. Therefore, the Dongyuemiao shale does not possess any significant disadvantages compared to the Da'anzhai shale, and it should be given more attention in future exploration efforts.

Author Contributions: Conceptualization, E.W.; Data curation, T.G.; Writing—original draft, E.W.; Writing—review & editing, Y.L., T.G., L.X., X.D., T.W. and K.S. All authors have read and agreed to the published version of the manuscript.

Funding: This study is supported by the open fund of the State Key Laboratory of Shale Oil and Gas Enrichment Mechanisms and Effective Development (Project No. 33550000-22-ZC0613-0337) and the fund of Sinopec Science and Technology (P22122, P23102-05).

Data Availability Statement: Data is contained within the article.

Conflicts of Interest: The authors declare no conflict of interest.

References

1. Guo, T.L. Key controls on accumulation and high production of large non-marine gas fields in northern Sichuan Basin. *Petrol. Explor. Dev.* **2013**, *40*, 139–149. [CrossRef]
2. Hu, T.; Pang, X.Q.; Jiang, S.; Wang, Q.F.; Zheng, X.W.; Ding, X.G.; Zhao, Y.; Zhu, C.X.; Li, H. Oil content evaluation of lacustrine organic-rich shale with strong heterogeneity: A case study of the Middle Permian Lucaogou Formation in Jimusaer Sag, Junggar Basin, NW China. *Fuel* **2018**, *221*, 196–205. [CrossRef]
3. Li, C.R.; Pang, X.Q.; Huo, Z.P.; Wang, E.Z.; Xue, N. A revised method for reconstructing the hydrocarbon generation and expulsion history and evaluating the hydrocarbon resource potential: Example from the first member of the Qingshankou Formation in the Northern Songliao Basin, Northeast China. *Mar. Pet. Geol.* **2020**, *121*, 104577. [CrossRef]
4. Liu, B.; Sun, J.H.; Zhang, Y.Q.; He, J.L.; Fu, X.F.; Yang, L.; Xing, J.L.; Zhao, X.P. Reservoir space and enrichment model of shale oil in the first member of Cretaceous Qingshankou Formation in the Changling Sag, southern Songliao Basin, NE China. *Petrol. Explor. Dev.* **2021**, *48*, 608–624. [CrossRef]
5. Pang, X.Q.; Li, M.; Li, B.Y.; Wang, T.; Hui, S.S.; Liu, Y.; Liu, G.Y.; Hu, T.; Xu, T.W.; Jiang, F.J.; et al. Main controlling factors and movability evaluation of continental shale oil. *Earth-Sci. Rev.* **2023**, *243*, 104472.
6. Li, J.B.; Wang, M.; Jiang, C.Q.; Lu, S.F.; Li, Z. Sorption model of lacustrine shale oil: Insights from the contribution of organic matter and clay minerals. *Energy* **2022**, *260*, 125011. [CrossRef]
7. Ma, Y.S.; Cai, X.Y.; Zhao, P.R.; Hu, Z.Q.; Liu, H.M.; Gao, B.; Wang, W.Q.; Li, Z.M.; Zhang, Z.L. Geological characteristics and exploration practices of continental shale oil in China. *Acta Geol. Sin.* **2022**, *96*, 155–171, (In Chinese with English Abstract).
8. Wang, E.Z.; Feng, Y.; Guo, T.L.; Li, M.W. Oil content and resource quality evaluation methods for lacustrine shale: A review and a novel three-dimensional quality evaluation model. *Earth-Sci. Rev.* **2022**, *232*, 104134. [CrossRef]
9. Wang, E.Z.; Li, C.R.; Feng, Y.; Song, Y.C.; Guo, T.L.; Li, M.W.; Chen, Z.H. Novel method for determining the oil moveable threshold and an innovative model for evaluating the oil content in shales. *Energy* **2022**, *239*, 121848. [CrossRef]
10. Wang, E.Z.; Guo, T.L.; Li, M.W.; Xiong, L.; Dong, X.X.; Wang, T.; Ouyang, J.S. Reservoir characteristics and oil properties of a lacustrine shale system: Early Jurassic black shale from the Sichuan Basin, SW China. *J. Asian Earth Sci.* **2023**, *242*, 105491. [CrossRef]
11. Wang, E.Z.; Guo, T.L.; Li, M.W.; Xiong, L.; Dong, X.X.; Wang, T.; Li, H.Q. Favorable Exploration Lithofacies and Their Formation Mechanisms in Lacustrine Shales Deposited under Different Salinity Conditions: Insights into Organic Matter Accumulation and Pore Systems. *Energy Fuels* **2023**, *37*, 11838–11852. [CrossRef]
12. Jin, Z.J. Hydrocarbon accumulation and resources evaluation: Recent advances and current challenges. *Adv. Geo-Energy Res.* **2023**, *8*, 1–4. [CrossRef]
13. Hu, T.; Wu, G.Y.; Xu, Z.; Pang, X.Q.; Liu, Y.; Yu, S. Potential resources of conventional, tight, and shale oil and gas from Paleogene Wenchang Formation source rocks in the Huizhou Depression. *Adv. Geo-Energy Res.* **2022**, *6*, 402–414. [CrossRef]
14. Zou, C.N.; Dong, D.Z.; Wang, Y.M.; Li, X.J.; Huang, J.L.; Wang, S.F.; Guan, Q.Z.; Zhang, C.C.; Wang, H.Y.; Liu, H.L.; et al. Shale gas in China: Characteristics, challenges and prospects (II). *Petrol. Explor. Dev.* **2016**, *43*, 166–178. [CrossRef]
15. Guo, X.S.; Hu, D.F.; Li, Y.P.; Wei, Z.H.; Wei, X.F.; Liu, Z.J. Geological factors controlling shale gas enrichment and high production in Fuling shale gas field. *Petrol. Explor. Dev.* **2017**, *44*, 481–491. [CrossRef]
16. Wang, Y.F.; Zhai, G.Y.; Liu, G.H.; Shi, W.Z.; Lu, Y.C.; Li, J.; Zhang, Y.X. Geological Characteristics of Shale Gas in Different Strata of Marine Facies in South China. *J. Earth Sci.* **2021**, *32*, 725–741. [CrossRef]
17. Liu, G.H.; Liu, B.; Liu, K.Y.; Zhai, G.Y.; Guo, Z.G. Silica crystallinity: Characteristics and controlling factors in marine shale of the upper Yangtze area, China. *Mar. Pet. Geol.* **2022**, *151*, 105833. [CrossRef]
18. Feng, Y.; Xiao, X.M.; Gao, P.; Wang, E.Z.; Hu, D.F.; Liu, R.B.; Li, G.; Lu, C.G. Restoration of sedimentary environment and geochemical features of deep marine Longmaxi shale and its significance for shale gas: A case study of the Dingshan area in the Sichuan Basin, South China. *Mar. Pet. Geol.* **2023**, *151*, 106186. [CrossRef]
19. Zou, C.N.; Yang, Z.; Zhao, Q.; Bai, W.H.; Liu, H.L.; Pan, S.Q.; Wu, S.T.; Yuan, Y.L. "Exploring petroleum inside source kitchen": Shale oil and gas in Sichuan Basin. *Sci. China Earth Sci.* **2020**, *63*, 934–953. [CrossRef]
20. Zhang, P.; Wang, Y.; Zhang, X.; Wei, Z.; Wang, G.; Zhang, T.; Ma, H.; Wei, J.; He, W.; Ma, X.; et al. Carbon, oxygen and strontium isotopic and elemental characteristics of the Cambrian Longwangmiao Formation in South China: Paleoenvironmental significance and implications for carbon isotope excursions. *Gondwana Res.* **2022**, *106*, 174–190.
21. Zhang, P.; Wang, Y.; Wei, Z.; Wang, G.; Zhang, T.; He, W.; Ma, X.Y.; Ma, H.; Wei, J.Y.; Zhu, C.X. Influence of the late Ordovician-early Silurian paleoenvironment and related geological processes on the organic matter accumulation and carbon isotope excursion. *Paleoceanogr. Paleoclimatology* **2023**, *38*, e2023PA004628. [CrossRef]
22. Yang, J.Q.; Zhang, J.T.; He, Z.L.; Zhang, T. Paleoenvironment reconstruction of the Middle Ordovician thick carbonate from western Ordos Basin, China. *Pet. Sci.* **2023**, *20*, 48–59. [CrossRef]
23. Liu, M.; Sun, P.; Them II, T.R.; Li, Y.F.; Sun, S.L.; Gao, X.Y.; Huang, X.; Tang, Y.J. Organic geochemistry of a lacustrine shale across the Toarcian Oceanic Anoxic Event (Early Jurassic) from NE China. *Glob. Planet. Change* **2020**, *191*, 103214. [CrossRef]
24. Jin, X.; Shi, Z.Q.; Baranyi, V.; Kemp, D.B.; Han, Z.; Luo, G.M.; Hu, J.F.; He, F.; Chen, L.; Preto, N. The Jenkyns Event (early Toarcian OAE) in the Ordos Basin, North China. *Glob. Planet. Chang.* **2020**, *193*, 103273. [CrossRef]
25. Fu, X.P.; Yang, T. Pore structure of continental shale reservoirs in Lower Jurassic Ziliujing Formation, northeastern Sichuan Basin. *Pet. Geol. Exp.* **2021**, *43*, 589–598.

26. Qiu, Z.; He, J.L. Depositional environment changes and organic matter accumulation of Pliensbachian-Toarcian lacustrine shales in the Sichuan basin, SW China. *J. Asian Earth Sci.* **2022**, *232*, 105035. [CrossRef]
27. Li, Y.J.; Feng, Y.Y.; Liu, H.; Zhang, L.H.; Zhao, S.X. Geological characteristics and resource potential of lacustrine shale gas in the Sichuan Basin, SW China. *Petrol. Explor. Dev.* **2013**, *40*, 423–428. [CrossRef]
28. Liu, S.G.; Yang, Y.; Deng, B.; Zhong, Y.; Wen, L.; Sun, W.; Li, Z.W.; Jansa, L.; Li, J.X.; Song, J.M.; et al. Tectonic evolution of the Sichuan Basin, Southwest China. *Earth-Sci. Rev.* **2021**, *213*, 103470. [CrossRef]
29. Wang, E.Z.; Guo, T.L.; Li, M.W.; Xiong, L.; Dong, X.X.; Zhang, N.X.; Wang, T. Depositional Environment Variation and Organic Matter Accumulation Mechanism of Marine–Continental Transitional Shale in the Upper Permian Longtan Formation, Sichuan Basin, SW China. *ACS Earth Space Chem.* **2022**, *6*, 2199–2214. [CrossRef]
30. Qiu, L.; Yan, D.P.; Tang, S.L.; Wang, Q.; Yang, W.X.; Tang, X.L.; Wang, J.B. Mesozoic geology of southwestern China: Indosinian foreland overthrusting and subsequent deformation. *J. Asian Earth Sci.* **2016**, *122*, 91–105. [CrossRef]
31. Shao, T.B.; Cheng, N.F.; Song, M.S. Provenance and tectonic-paleogeographic evolution: Constraints from detrital zircon U–Pb ages of Late Triassic-Early Jurassic deposits in the northern Sichuan basin, central China. *J. Asian Earth Sci.* **2016**, *127*, 12–31. [CrossRef]
32. Nie, H.K.; Jin, Z.J.; Li, P.; Katz, B.J.; Dang, W.; Liu, Q.Y.; Ding, J.H.; Jiang, S.; Li, D.H. Deep shale gas in the Ordovician-Silurian Wufeng–Longmaxi formations of the Sichuan Basin, SW China: Insights from reservoir characteristics, preservation conditions and development strategies. *J. Asian Earth Sci.* **2023**, *244*, 105521. [CrossRef]
33. Faure, M.; Lepvrier, C.; Nguyen, V.V.; Vu, T.V.; Lin, W.; Chen, Z.C. The South China block-Indochina collision: Where, when, and how? *J. Asian Earth Sci.* **2014**, *79*, 260–274. [CrossRef]
34. Halpin, J.A.; Tran, H.T.; Lai, C.K.; Meffre, S.; Crawford, A.J.; Zaw, K. U–Pb zircon geochronology and geochemistry from NE Vietnam: A 'tectonically disputed' territory between the Indochina and South China blocks. *Gondwana Res.* **2016**, *2016*, 254–273. [CrossRef]
35. Taylor, S.R.; McLennan, S.M. *The Continental Crust: Its Composition and Evolution*; Blackwell: Oxford, UK, 1985; p. 312.
36. Minyuk, P.S.; Brigham–Grette, J.; Melles, M.; Borkhodoev, V.Y.; Glushkova, O.Y. Inorganic geochemistry of El'gygytgyn Lake sediments (northeastern Russia) as an indicator of paleoclimatic change for the last 250 kyr. *J. Paleolimnol.* **2007**, *37*, 123–133. [CrossRef]
37. Nesbitt, H.W.; Young, G.M. Early Proterozoic climates and plate motions inferred from major element chemistry of lutites. *Nature* **1982**, *299*, 715–717. [CrossRef]
38. McLennan, S.M.; Hemming, S.; McDaniel, D.K.; Hanson, G.N. Geochemical approaches to sedimentation, provenance, and tectonics. *Geol. Soc. Am. Spec. Pap.* **1993**, *284*, 21–40.
39. Zhao, Z.Y.; Zhao, J.H.; Wang, H.J.; Liao, J.D.; Liu, C.M. Distribution characteristics and applications of trace elements in Junggar basin. *Nat. Gas Exp. Dev.* **2007**, *30*, 30–33, (In Chinese with English Abstract).
40. Loucks, R.G.; Reed, R.M.; Ruppel, S.C.; Jarvie, D.M. Morphology, genesis, and distribution of nanometer-scale pores in siliceous mudstones of the Mississippian Barnett Shale. *J. Sediment. Res.* **2009**, *79*, 848–861. [CrossRef]
41. Chen, L.; Jiang, Z.X.; Liu, Q.X.; Jiang, S.; Liu, K.Y.; Tan, J.Q.; Gao, F.L. Mechanism of shale gas occurrence: Insights from comparative study on pore structures of marine and lacustrine shales. *Mar. Pet. Geol.* **2019**, *104*, 200–216. [CrossRef]
42. Xia, G.Q.; Mansour, A. Paleoenvironmental changes during the early Toarcian Oceanic Anoxic Event: Insights into organic carbon distribution and controlling mechanisms in the eastern Tethys. *J. Asian Earth Sci.* **2022**, *237*, 105344. [CrossRef]
43. Wu, Z.Y.; Zhao, X.Z.; Wang, E.Z.; Pu, X.G.; Lash, G.; Han, W.Z.; Zhang, W.; Feng, Y. Sedimentary environment and organic enrichment mechanisms of lacustrine shale: A case study of the Paleogene Shahejie Formation, Qikou Sag, Bohai Bay Basin. *Palaeogeogr. Palaeoclimatol. Palaeoecol.* **2021**, *573*, 110404. [CrossRef]
44. Mansour, A.; Wagreich, M. Earth system changes during the cooling greenhouse phase of the Late Cretaceous: Coniacian-Santonian OAE3 subevents and fundamental variations in organic carbon deposition. *Earth-Sci. Rev.* **2022**, *229*, 104022. [CrossRef]
45. Scott, C.; Lyons, T.W. Contrasting molybdenum cycling and isotopic properties in euxinic versus non-euxinic sediments and sedimentary rocks: Refining the paleoproxies. *Chem. Geol.* **2012**, *324*, 19–27. [CrossRef]
46. Jones, B.; Manning, D.A. Comparison of geochemical indices used for the interpretation of palaeoredox conditions in ancient mudstones. *Chem. Geol.* **1994**, *111*, 111–129. [CrossRef]
47. Khanehbad, M.; Moussavi-Harami, R.; Mahboubi, A.; Nadjafi, M. Geochemistry of Carboniferous Shales of the Sardar Formation, East Central Iran: Implication for Provenance, Paleoclimate and Paleo-oxygenation Conditions at a Passive Continental Margin. *Geochem. Int.* **2012**, *50*, 867–880. [CrossRef]
48. Algeo, T.J.; Ingall, E. Sedimentary Corg: P ratios, paleocean ventilation, and Phanerozoic atmospheric pO_2. *Palaeogeogr. Palaeoclimatol. Palaeoecol.* **2007**, *256*, 130–155. [CrossRef]
49. Pan, Y.; Huang, Z.; Guo, X.; Wang, R.; Lash, G.G.; Fan, T.G.; Liu, W. A re-assessment and calibration of redox thresholds in the Permian Lucaogou Formation of the Malang Sag, Santanghu Basin, Northwest China. *Mar. Pet. Geol.* **2021**, *135*, 105406. [CrossRef]
50. Wei, W.; Algeo, T.J. Elemental proxies for paleosalinity analysis of ancient shales and mudrocks. *Geochim. Cosmochim. Acta* **2020**, *287*, 341–366. [CrossRef]

51. Tribovillard, N.; Desprairies, A.; Lallier-Vergès, E.; Bertrand, P.; Moureau, N.; Ramdani, A.; Ramanampisoa, L. Geochemical study of organic-matter rich cycles from the Kimmeridge Clay Formation of Yorkshire (UK): Productivity versus anoxia. *Palaeogeogr. Palaeoclimatol. Palaeoecol.* **1994**, *108*, 165–181. [CrossRef]
52. Nie, Y.; Fu, X.G.; Liang, J.T.; Wei, H.Y.; Chen, Z.G.; Lin, F.; Zeng, S.Q.; Wu, Y.H.; Zou, Y.; Mansour, A. The Toarcian Oceanic Anoxic Event in a shelf environment (Eastern Tethys): Implications for weathering and redox conditions. *Sediment. Geol.* **2023**, *455*, 106476. [CrossRef]
53. Reolid, M.; Rodriguez-Tovar, F.J.; Marok, A.; Sebane, A. The Toarcian oceanic anoxic event in the Western Saharan Atlas, Algeria (North African paleomargin): Role of anoxia and productivity. *Geol. Soc. Am. Bull.* **2012**, *124*, 1646–1664. [CrossRef]
54. Tribovillard, N.; Algeo, T.J.; Lyons, T.; Riboulleau, A. Trace metals as paleoredox and paleoproductivity proxies: An update. *Chem. Geol.* **2006**, *232*, 12–32. [CrossRef]
55. Kennedy, M.J.; Pevear, D.R.; Hill, R.J. Mineral surface control of organic carbon in black shale. *Science* **2002**, *295*, 657–660. [CrossRef]
56. Ricken, W. Bedding rhythms and cyclic sequences as documented in organic carbon-carbonate patterns, Upper Cretaceous, Western Interior, U.S. *Sediment. Geol.* **1996**, *102*, 131–154. [CrossRef]
57. Tyson, R.V. Sedimentation rate, dilution, preservation and total organic carbon: Some results of a modelling study. *Org. Geochem.* **2001**, *32*, 333–339. [CrossRef]
58. Yang, G.Q.; Zeng, J.H.; Qiao, J.C.; Liu, Y.Z.; Liu, S.N.; Jia, W.T.; Cao, W.F.; Wang, C.Y.; Geng, F.; Wei, W.F. Role of organic matter, mineral, and rock fabric in the full-scale pore and fracture network development in the mixed lacustrine source rock system. *Energy Fuels* **2022**, *36*, 8161–8179. [CrossRef]
59. Wang, E.Z.; Feng, Y.; Guo, T.L.; Li, M.W.; Xiong, L.; Lash, G.G.; Dong, X.X.; Wang, T.; Ouyang, J.S. Sedimentary differentiation triggered by the Toarcian Oceanic Anoxic Event and formation of lacustrine shale oil reservoirs: Organic matter accumulation and pore system evolution of the Early Jurassic sedimentary succession, Sichuan Basin, China. *J. Asian Earth Sci.* **2023**, *256*, 105825. [CrossRef]
60. He, W.Y.; Bai, X.F.; Meng, Q.A.; Li, J.H.; Zhang, D.Z.; Wang, Y.Z. Accumulation geological characteristics and major discoveries of lacustrine shale oil in Sichuan Basin. *Acta Pet. Sin.* **2022**, *43*, 886–898. (In Chinese with English Abstract)